

Evidence for widespread thermal optimality of ecosystem respiration

Received: 31 July 2022

Accepted: 16 June 2023

Published online: 24 July 2023

 Check for updates

Weinan Chen^{1,2}, Song Wang^{1,2}, Jinsong Wang¹, Jianyang Xia³, Yiqi Luo⁴, Guirui Yu^{1,2} & Shuli Niu^{1,2}✉

Ecosystem respiration (ER) is among the largest carbon fluxes between the biosphere and the atmosphere. Understanding the temperature response of ER is crucial for predicting the climate change–carbon cycle feedback. However, whether there is an apparent optimum temperature of ER ($T_{\text{opt}}^{\text{ER}}$) and how it changes with temperature remain poorly understood. Here we analyse the temperature response curves of ER at 212 sites from global FLUXNET. We find that ER at 183 sites shows parabolic temperature response curves and $T_{\text{opt}}^{\text{ER}}$ at which ER reaches the maximum exists widely across biomes around the globe. Among the 15 biotic and abiotic variables examined, $T_{\text{opt}}^{\text{ER}}$ is mostly related to the optimum temperature of gross primary production (GPP, $T_{\text{opt}}^{\text{GPP}}$) and annual maximum daily temperature (T_{max}). In addition, $T_{\text{opt}}^{\text{ER}}$ linearly increases with T_{max} across sites and over vegetation types, suggesting its thermal adaptation. The adaptation magnitude of $T_{\text{opt}}^{\text{ER}}$, which is measured by the change in $T_{\text{opt}}^{\text{ER}}$ per unit change in T_{max} , is positively correlated with the adaptation magnitude of $T_{\text{opt}}^{\text{GPP}}$. This study provides evidence of the widespread existence of $T_{\text{opt}}^{\text{ER}}$ and its thermal adaptation with T_{max} across different biomes around the globe. Our findings suggest that carbon cycle models that consider the existence of $T_{\text{opt}}^{\text{ER}}$ and its adaptation have the potential to more realistically predict terrestrial carbon sequestration in a world with changing climate.

Ecosystem respiration (ER) is a major component of carbon exchanges between terrestrial ecosystems and the atmosphere, plays an important role in determining the carbon balance of an ecosystem and affects atmospheric carbon dioxide (CO₂) concentration^{1,2}. Temperature substantially influences respiratory CO₂ emission^{3,4}. Understanding the long-term responses and adaptation of ER to temperature is critical to improving model prediction of ecosystem carbon cycling under future climate warming^{5–10}.

However, our understanding of the temperature responses of ER remains limited, partly because ER is a sum of complex processes of autotrophic and heterotrophic respiration affected by many confounding factors^{11,12}. The temperature response of leaf respiration is

generally exponential over a broad range of temperatures¹³. However, more and more recent studies have demonstrated that leaf respiration reaches a peak at a maximum temperature, followed by a sharp decline at higher temperatures^{6,14–19}. On the other hand, the thermodynamic properties of enzymes²⁰, the short supply of respiratory substrates^{13,21} and thermal adaptation of microbial growth²² may all lead to a decline in both auto- and heterotrophic respiration at high temperatures. Thus, these mechanisms individually or in combination could potentially result in a parabolic temperature response curve of ecosystem respiration with an optimum temperature ($T_{\text{opt}}^{\text{ER}}$). Investigating the existence of a temperature optimum for respiration at the ecosystem level for various biomes and how it changes with environmental factors

¹Key Laboratory of Ecosystem Network Observation and Modeling, Institute of Geographic Sciences and Natural Resources Research, Chinese Academy of Sciences, Beijing, P. R. China. ²College of Resources and Environment, University of Chinese Academy of Sciences, Beijing, P. R. China. ³Research Center for Global Change and Complex Ecosystems, East China Normal University, Shanghai, China. ⁴School of Integrative Plant Science, Cornell University, Ithaca, NY, USA. ✉e-mail: sniu@igsnr.ac.cn

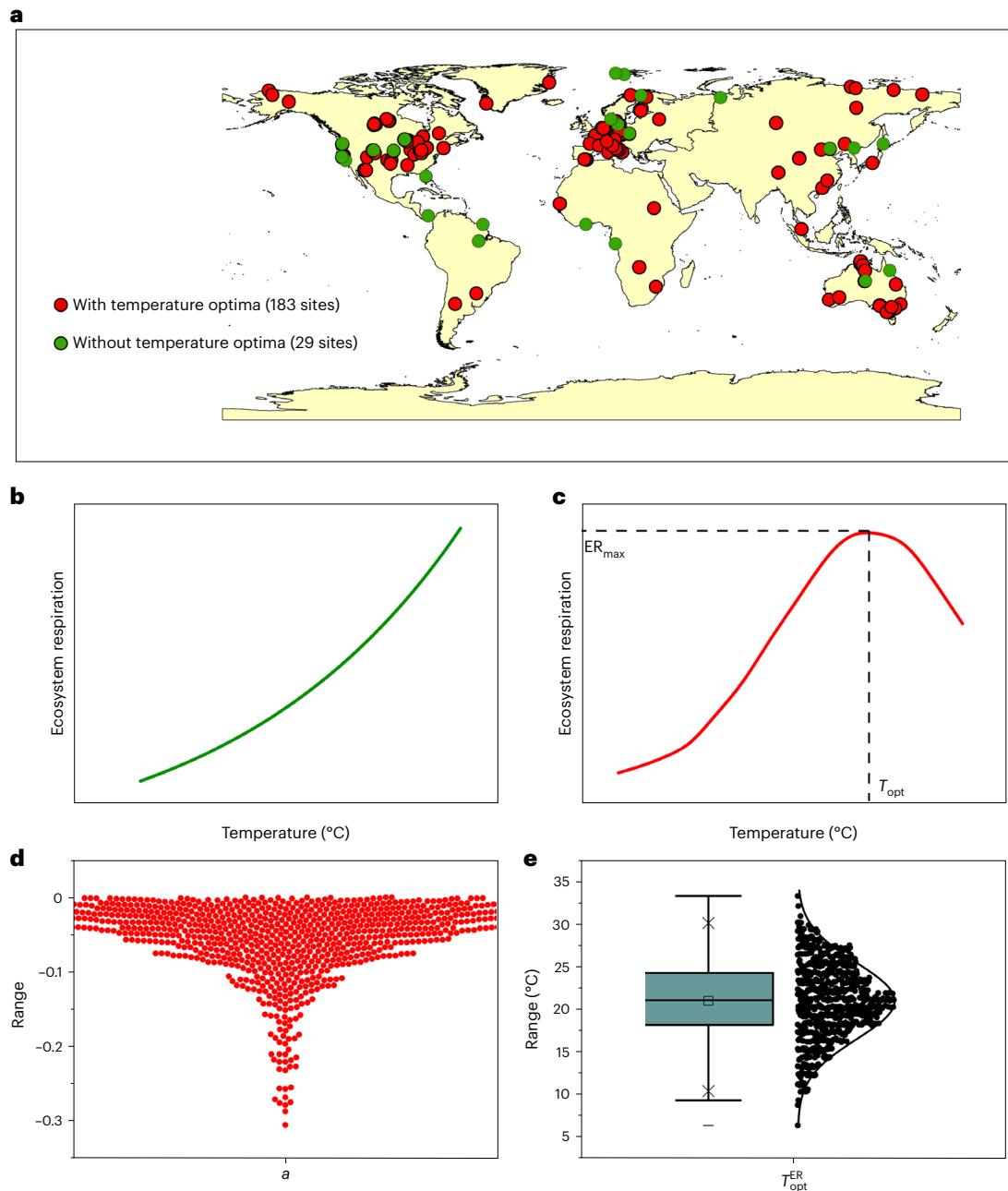


Fig. 1 | Distribution of $T_{\text{opt}}^{\text{ER}}$ derived from flux-tower sites. a, Location of the 183 FLUXNET sites (red circles) used in this study with detected temperature optima for ER and the 29 FLUXNET sites (green circles) excluded from this study without detected temperature optima for ER. **b**, The response of ER to temperature in an exponential function without temperature optima. **c**, The response of ER to temperature in a single-peak function with temperature optima. **d**, Parameter estimate of the fitted quadratic function at $T_{\text{opt}}^{\text{ER}}$ for the 183 sites with temperature optima. a is the parameter estimate of the fitted quadratic function at $T_{\text{opt}}^{\text{ER}}$ (equation 1). Negative values indicate that the curve is concave, large values

indicate strong curvature (that is, sharp curves) and small values indicate weak curvature (that is, flat curves). Here we used a beeswarm plot to show the distribution of parameter a . A beeswarm plot is a one-dimensional scatterplot similar to a 'stripchart' and is a good way of showing the distribution of a given variable while also showing each individual data point. **e**, Distribution of $T_{\text{opt}}^{\text{ER}}$ ($n = 183$). Whiskers, maximum and minimum values; top, middle and bottom lines of the box: 75% quantile, median and 25% quantile; square in box, mean value; crosses (x), 1% and 99% quantiles; points and curve on the right, normal distribution of $T_{\text{opt}}^{\text{ER}}$

are valuable for accurately predicting the climate change–carbon cycle feedback.

In comparison, plant photosynthetic rates have been well documented to increase with temperature, reaching an optimum temperature above which photosynthetic rates decline^{7,23–27}. The optimum temperature of plant photosynthesis ($T_{\text{opt}}^{\text{GPP}}$) usually varies over space, being higher in a warmer environment at both leaf and ecosystem scales for a wide range of plant species and plant

functional types^{27,28}. This variation in $T_{\text{opt}}^{\text{GPP}}$ with temperature is probably a result of thermal adaptation. On the other hand, both heterotrophic and autotrophic respiratory fluxes are closely coupled with photosynthesis via their dependence on photosynthetic substrate supply^{29–35}. Notably, the connection of plant respiration with photosynthesis is tight as reported in many previous studies^{36–43}. It is likely that plants thermally adapt photosynthesis and respiration in a coordinated fashion^{44,45}. In this sense, changes in the response of

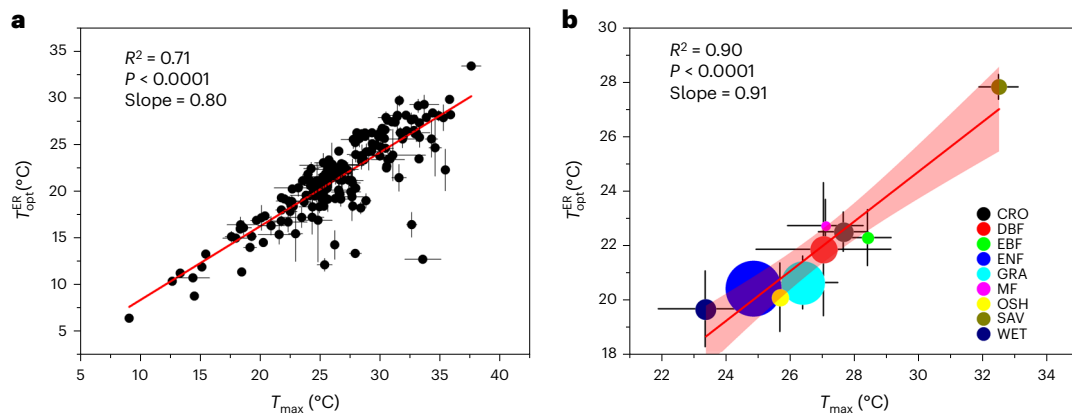


Fig. 2 | The relationship of $T_{\text{opt}}^{\text{ER}}$ to T_{max} . **a**, Relationship across sites ($n = 183$) and vegetation types (**b**) ($n = 9$). Red lines represent the significant linear regression relationship across sites and vegetation types. Circle size is proportional to the number of sites in each ecosystem type. Circles and error bars

indicate mean \pm s.d. CRO, cropland, $n = 17$; DBF, deciduous broadleaf forests, $n = 22$; EBF, evergreen broadleaf forest, $n = 10$; ENF, evergreen needle-leaf forest, $n = 45$; GRA, grassland, $n = 35$; MF, mixed forest, $n = 8$; OSH, open shrublands, $n = 14$; WET, wetland, $n = 17$; SAV, savanna, $n = 13$. Shaded areas represent 95% CIs (F -test).

respiration to temperature might be closely related to adjustments in the response of photosynthesis to temperature, or might even adjust faster than photosynthesis at the ecosystem scale⁴⁶. Thus, $T_{\text{opt}}^{\text{ER}}$, if it exists, probably shifts higher with higher temperatures as $T_{\text{opt}}^{\text{GPP}}$ does in a warmer climate.

Furthermore, it is of great importance to understand how the variation in $T_{\text{opt}}^{\text{ER}}$ will affect annual ER for an accurate estimation of ER in a changing climate. Thus, it is crucial to investigate the effects of $T_{\text{opt}}^{\text{ER}}$ on ER in addition to examining the existence of $T_{\text{opt}}^{\text{ER}}$ in different ecosystems, its thermal adaptation across sites and biomes, and the relationships between $T_{\text{opt}}^{\text{ER}}$ and $T_{\text{opt}}^{\text{GPP}}$. The relationship between $T_{\text{opt}}^{\text{ER}}$ and ER can help us better understand how climatic warming impacts ecosystem carbon fluxes.

In this study, we analysed the temperature response curves of independently estimated ER and gross primary production (GPP) from the FLUXNET datasets at 212 sites. The specific hypotheses we tested in this study are: (1) $T_{\text{opt}}^{\text{ER}}$ exists in most biomes; (2) $T_{\text{opt}}^{\text{ER}}$ increases with temperature across sites and over vegetation types; (3) $T_{\text{opt}}^{\text{ER}}$ is mostly related to $T_{\text{opt}}^{\text{GPP}}$ and annual maximum daily temperature (T_{max}) rather than other influencing factors, and its adaptation magnitude is correlated with that of $T_{\text{opt}}^{\text{GPP}}$; and (4) $T_{\text{opt}}^{\text{ER}}$ largely determines annual ER across sites globally.

Results

Existence of $T_{\text{opt}}^{\text{ER}}$

We detected the existence of an apparent optimum temperature of ER ($T_{\text{opt}}^{\text{ER}}$) at 183 sites covering large areas and most vegetation types from a total of 212 sites in our dataset (Fig. 1a–c). Quantitative analysis showed that all the temperature response curves of ER at these sites followed significant concave quadratic functions rather than exponential functions with air temperature (T_a) (Fig. 1d, Extended Data Figs. 1 and 2). Across the 183 sites, $T_{\text{opt}}^{\text{ER}}$ ranged from 6.5 to 33.3 °C (Fig. 1e). The residuals of ER– T_a curves did not have any significant relationship with soil moisture (SM), vapour pressure deficit (VPD), global radiation or leaf area index (LAI), suggesting that the existence of $T_{\text{opt}}^{\text{ER}}$ was not likely caused by these confounding factors (Supplementary Fig. 1). For the 29 sites where the parabolic curves were not found and a $T_{\text{opt}}^{\text{ER}}$ was thus absent, we found that this absence was mainly due to two reasons. First, some tropical sites (seven sites) had little variation in seasonal temperature (<3 °C), which made it difficult to generate any clear response curves (Supplementary Information 2). Second, 22 sites had GPPs not reaching optimum temperature (Supplementary Fig. 2).

Dependence of $T_{\text{opt}}^{\text{ER}}$ on $T_{\text{opt}}^{\text{GPP}}$ and T_{max}

$T_{\text{opt}}^{\text{ER}}$ values across sites were positively correlated with the annual maximum daily air temperature (T_{max}) ($R^2 = 0.71$, $P < 0.001$), with a spatial linear regression slope of 0.80 °C per °C across sites (Fig. 2a). This thermal adaptation of $T_{\text{opt}}^{\text{ER}}$ to T_{max} was also observed across different vegetation types (Fig. 2b), with a spatial linear regression slope of 0.91 °C per °C across biomes ($R^2 = 0.90$, $P < 0.001$). The slope indicates the thermal adaptation magnitude of ER to the local temperature.

Ridge regression was applied to disentangle the independent effects of the co-varying factors individually on $T_{\text{opt}}^{\text{ER}}$. It showed that $T_{\text{opt}}^{\text{ER}}$ was majorly determined by $T_{\text{opt}}^{\text{GPP}}$ and T_{max} , while other biotic and abiotic factors including biomass, mean annual temperature (MAT) or precipitation (MAP), aridity index (AI), VPD, growing season temperature (GST) or radiation (GSR), SM, soil pH (pH), soil organic carbon (SOC), clay fraction (Clay) and soil bulk density (BD) did not significantly influence $T_{\text{opt}}^{\text{ER}}$, although some of them were significant in the bivariate regression (Fig. 3a and Extended Data Fig. 3). $T_{\text{opt}}^{\text{ER}}$ shifted upwards with an increase in $T_{\text{opt}}^{\text{GPP}}$ across sites and biomes, with a slope of 0.81 °C per °C ($R^2 = 0.74$, $P < 0.001$) across sites and 0.84 °C per °C ($R^2 = 0.88$, $P < 0.001$) across biomes (Fig. 3b,c). Variation partitioning analysis further confirmed that variation in $T_{\text{opt}}^{\text{ER}}$ was mostly explained by the interactive effects of $T_{\text{opt}}^{\text{GPP}}$ and T_{max} (63%), with $T_{\text{opt}}^{\text{GPP}}$ having a slightly higher independent contribution than T_{max} (11% versus 8%) (Supplementary Fig. 4). The close relationships between $T_{\text{opt}}^{\text{ER}}$ and T_{max} and between $T_{\text{opt}}^{\text{ER}}$ and $T_{\text{opt}}^{\text{GPP}}$ also existed over years within sites (Extended Data Fig. 4). Meanwhile, most of the sites without detected $T_{\text{opt}}^{\text{ER}}$ were accompanied by the absence of $T_{\text{opt}}^{\text{GPP}}$ data (Supplementary Fig. 2).

Defined as the positive spatial slope of the $T_{\text{opt}}^{\text{ER}}-T_{\text{max}}$ or $T_{\text{opt}}^{\text{GPP}}-T_{\text{max}}$ regression, the adaptation magnitude of $T_{\text{opt}}^{\text{ER}}$ was closely related to the adaptation magnitude of $T_{\text{opt}}^{\text{GPP}}$ across different vegetation types (Fig. 4; $R^2 = 0.55$, $P < 0.05$; Extended Data Fig. 5 and Supplementary Table 3).

A quadratic function was found between $T_{\text{opt}}^{\text{ER}}$ and annual ER (Fig. 5). There was a significant increase in the annual ER ($P < 0.05$) across sites when $T_{\text{opt}}^{\text{ER}}$ was below 21.0 °C. Above 21.0 °C, the annual ER decreased with $T_{\text{opt}}^{\text{ER}}$ at a relatively slower rate per °C ($P < 0.05$; Fig. 5).

Projection of $T_{\text{opt}}^{\text{ER}}$

We further established an empirical model to upscale $T_{\text{opt}}^{\text{ER}}$ using T_{max} , GST, VPD and BD on the basis of the stepwise regression model (Supplementary Table 5). Two thirds of the 183 sites were used for model fitting, and the remaining data were used for model validation (Extended Data Fig. 6). The empirical model explained more than 70% of the variation in $T_{\text{opt}}^{\text{ER}}$ across the global sites (Extended Data Fig. 6).

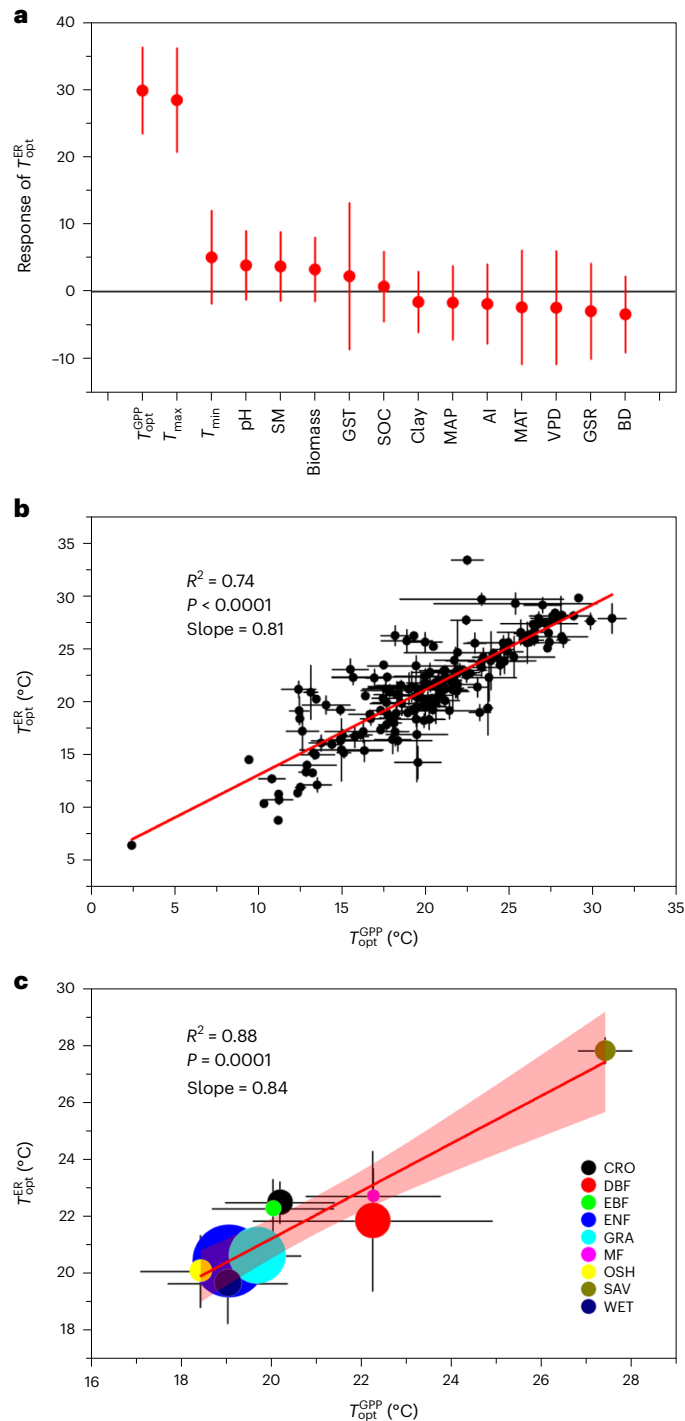


Fig. 3 | The relationship between T_{opt}^{ER} and influencing factors. **a**, The response of T_{opt}^{ER} to influencing variables estimated by ridge regression ($n = 183$). Circles represent the standardized coefficient of ridge regression between T_{opt}^{ER} and each of the variables; bars indicate 95% CIs. The influencing variables are: T_{opt}^{GPP} (°C); T_{max} (°C); T_{min} (°C); MAT (°C); GSR ($W m^{-2}$); MAP ($mm yr^{-1}$); GST (°C); VPD (kPa); SM; AI. **b, c**, Relationship between T_{opt}^{ER} and T_{opt}^{GPP} (F -test with 95% CIs) across sites (**b**) ($n = 183$) and vegetation types (**c**) ($n = 9$). Circle size is proportional to the number of sites in each ecosystem type. Circles and error bars indicate mean \pm s.d. CRO $n = 17$; DBF $n = 22$; EBF $n = 10$; ENF $n = 45$; GRA $n = 35$; MF $n = 8$; OSH $n = 14$; WET $n = 17$; SAV $n = 13$. Shaded areas represent 95% CIs.

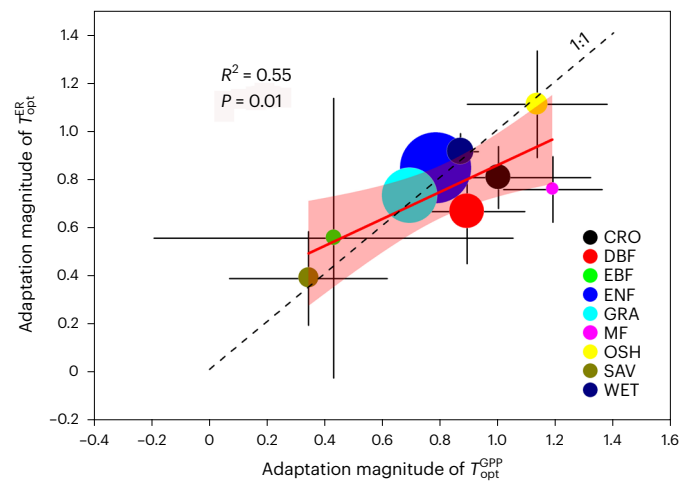


Fig. 4 | Relationship between the thermal adaptation magnitudes of T_{opt}^{GPP} and T_{opt}^{ER} across different vegetation types. The thermal adaptation magnitude represents the vegetation's capability to keep pace with temperature changes. Thermal adaptation magnitudes (including its 95% CI) less than 1 indicate that the T_{opt}^{ER} or T_{opt}^{GPP} of these vegetation types cannot fully adapt to T_{max} . Adaptation magnitudes and their 95% CIs including 1 indicate that the T_{opt}^{ER} or T_{opt}^{GPP} of these vegetation types can fully adapt to T_{max} . The red line depicts the relationship between the thermal adaptation magnitudes of T_{opt}^{GPP} and T_{opt}^{ER} (F -test with 95% CIs). The dashed line represents the 1:1 line. Circle size is proportional to the number of sites in each ecosystem type. Circles and error bars indicate mean \pm 95% CI. CRO $n = 17$; DBF $n = 22$; EBF $n = 10$; ENF $n = 45$; GRA $n = 35$; MF $n = 8$; OSH $n = 14$; WET $n = 17$; SAV $n = 13$. Shaded areas represent 95% CIs ($n = 9$).

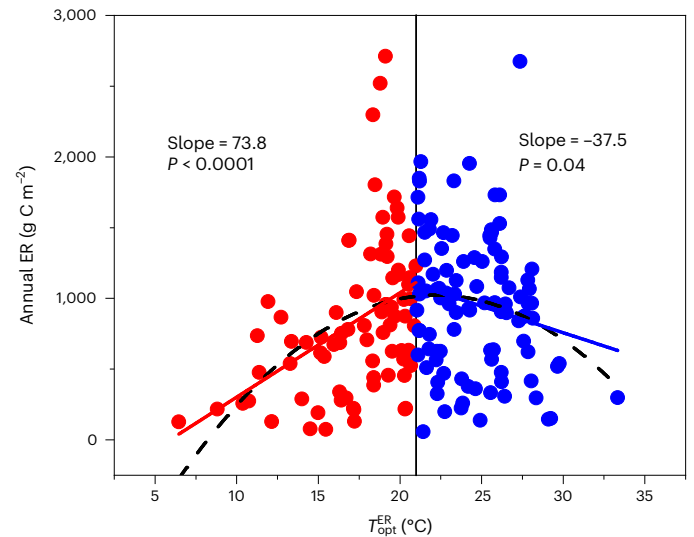


Fig. 5 | The relationship between annual ER and T_{opt}^{ER} . The red circles ($n = 79$) represent sites with T_{opt}^{ER} below the threshold of 21.0 °C, while the blue circles represent sites with T_{opt}^{ER} above the threshold of 21.0 °C ($n = 104$). The black dashed line represents a quadratic function between T_{opt}^{ER} and annual ER (F -test with 95% CI). The threshold of 21.0 °C is the vertex of the quadratic function. The red line represents positive linear relationship between T_{opt}^{ER} and annual ER for red points below the threshold, and the blue line represents negative linear relationship between T_{opt}^{ER} and annual ER for blue points above the threshold (F -test with 95% CI).

We then estimated T_{opt}^{ER} at present (2001–2010) and for the end of the century (2091–2100) under the SSP2–4.5 scenario at the global scale using this empirical model. At present, the maximum T_{opt}^{ER} values of

nearly 30 °C mainly appear over tropical forests, savannas and drylands, and the minimum values of near 10 °C prevail at high latitudes and in mountainous regions such as the Qinghai-Tibetan Plateau (Fig. 6a). By the end of this century, the global mean T_{opt}^{ER} increases from 22.6 to

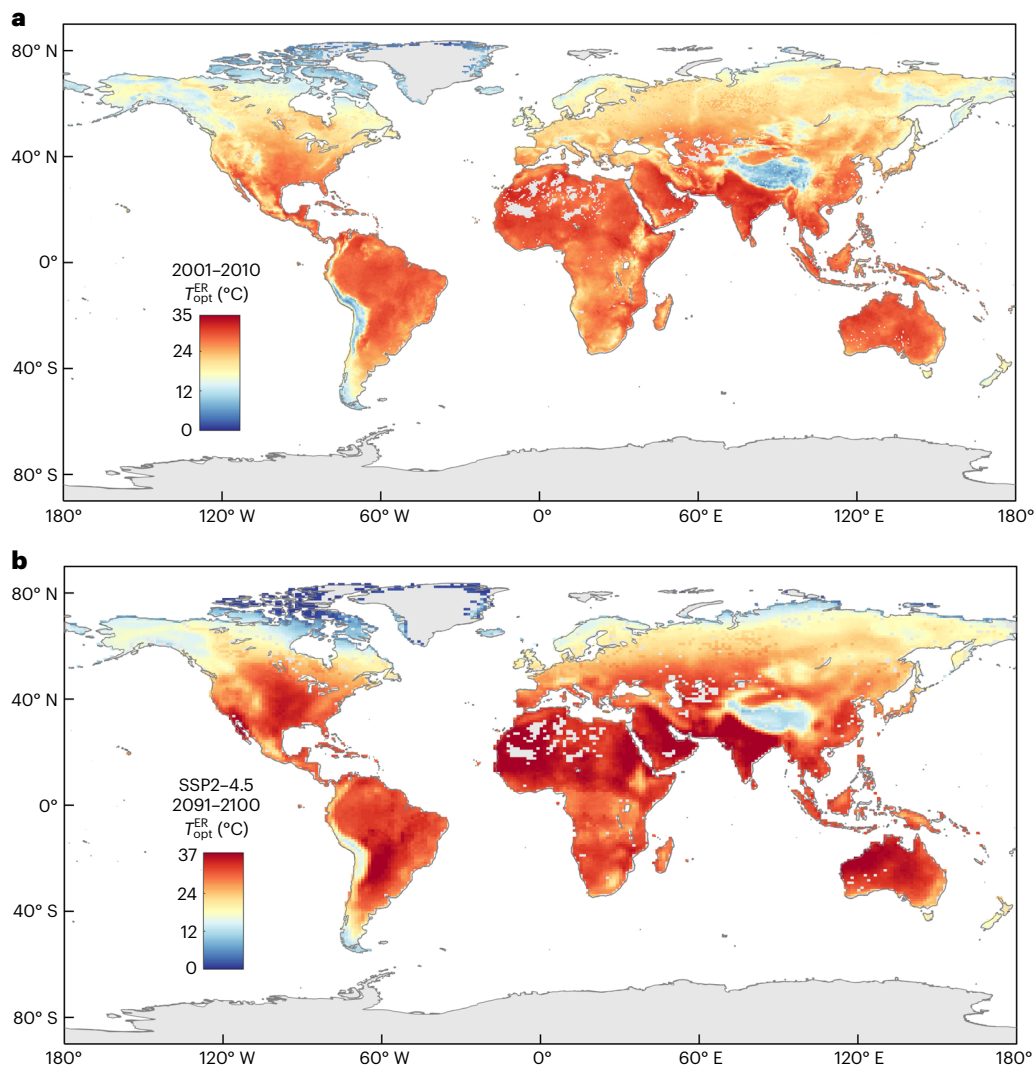


Fig. 6 | Projections of $T_{\text{opt}}^{\text{ER}}$. **a**, Current $T_{\text{opt}}^{\text{ER}}$. **b**, Future $T_{\text{opt}}^{\text{ER}}$ under the SSP2–4.5 scenario. T_{max} , GST, VPD and BD were used to predict $T_{\text{opt}}^{\text{ER}}$ on the basis of an empirical model in Supplementary Table 5. Current $T_{\text{opt}}^{\text{ER}}$ was calculated using current climate variables for 2001–2010 and future $T_{\text{opt}}^{\text{ER}}$ using climate variables for 2091–2100, projected by the NorESM2-MM model under the SSP2–4.5 scenario.

26.0 °C due to the higher T_{max} increasing from 25.5 to 29.3 °C (Fig. 6b). The standard deviation of the global $T_{\text{opt}}^{\text{ER}}$ ranges from 1.5 to 4.5 °C, with the largest uncertainty in North Africa, West Asia and South Asia (Extended Data Fig. 7).

Discussion

In this study, we detected the optimum temperature for ecosystem respiration ($T_{\text{opt}}^{\text{ER}}$) at 183 out of 212 sites across most of the ecosystem types over large geographical areas (37.4° S to 74.5° N) (Fig. 1). The widespread $T_{\text{opt}}^{\text{ER}}$ confirmed our first hypothesis that an apparent optimum temperature for ER exists in most of the biomes. It is clear that exponential response curves are not the best function to represent the relationship between temperature and ecosystem respiration over the season^{16,47,48} (Fig. 1 and Extended Data Fig. 1). The existence of $T_{\text{opt}}^{\text{ER}}$ is probably due to multiple mechanisms, such as the reduced supply of photosynthetic substrates and cell disruption or lysis of mitochondria at high temperatures, causing a decrease in leaf respiration^{13,15}. In addition, respiratory enzyme capacity and microbial growth is limited under high temperatures^{20,49}, which may also constrain heterotrophic respiration at high temperatures. Widespread $T_{\text{opt}}^{\text{ER}}$ also implies that terrestrial ecosystem respiration rates might sharply decline similar to

photosynthesis, instead of continuing to rise at higher temperatures⁵⁰. Hence, ignoring the existence of $T_{\text{opt}}^{\text{ER}}$ and its adaptation to higher temperatures in Earth system models can result in gross overestimation of the positive feedbacks between climate warming and terrestrial ecosystem carbon release^{6,8,14,44,47,51}.

The tight relationship between $T_{\text{opt}}^{\text{ER}}$ and T_{max} supports our second hypothesis that $T_{\text{opt}}^{\text{ER}}$ increases proportionally to T_{max} across sites and over vegetation types, which is similar to the relationship of $T_{\text{opt}}^{\text{ER}}$ to $T_{\text{opt}}^{\text{GPP}}$ (Fig. 2)^{13,28}. Our results demonstrated that the shift in the apparent optimum temperature is an emergent trait to represent ER thermal adaptation. In addition, both the ridge regression and bivariate regression analyses showed that the influence of $T_{\text{opt}}^{\text{GPP}}$ and T_{max} on $T_{\text{opt}}^{\text{ER}}$ dominates the effect of other biotic and abiotic factors (Fig. 3 and Extended Data Fig. 3). This result is consistent with our third hypothesis. The close relationship between $T_{\text{opt}}^{\text{ER}}$ and $T_{\text{opt}}^{\text{GPP}}$ across years within sites and the accompanying absence of $T_{\text{opt}}^{\text{GPP}}$ in most no- $T_{\text{opt}}^{\text{ER}}$ sites further confirmed the linkage between $T_{\text{opt}}^{\text{ER}}$ and $T_{\text{opt}}^{\text{GPP}}$ (Extended Data Fig. 4 and Supplementary Fig. 2). Our results add to the growing evidence that thermal adaptations of plant photosynthesis and respiration are coordinated^{44,45}. Moreover, our results expand the knowledge on adaptation coordination from the leaf scale to the ecosystem scale. However,

questions remain on what mechanisms promote the thermal optimality of ecosystem respiration when autotrophic respiration and heterotrophic respiration have different temperature responses and divergent links with photosynthesis.

We further quantified the thermal adaptation magnitude of ER by calculating the shift in $T_{\text{opt}}^{\text{ER}}$ in response to the change in T_{max} across large geographical gradients. The adaptation magnitude varied among different vegetation types (Extended Data Fig. 5), attributable to differences in interspecific variability in adaptation and climatic preferences⁴². Notably, the adaptation magnitude of savanna and evergreen broadleaf forest in $T_{\text{opt}}^{\text{ER}}$ was significantly lower than that of other ecosystem types, which is consistent with the notion that warmer ecosystems might have less adaptation capacity and less benefits under future warming compared with cooler ecosystems^{13,52} (Extended Data Fig. 5 and Supplementary Table 3). Meanwhile, the adaptation magnitude of $T_{\text{opt}}^{\text{ER}}$ was tightly related to the adaptation magnitude of $T_{\text{opt}}^{\text{GPP}}$ across different vegetation types (Figs. 4 and 5). This result further supported our conclusion that the thermal adaptations of photosynthesis and respiration are closely correlated. The closely correlated optimum temperature and adaptation magnitude between ER and GPP may contribute to homeostasis for ecosystem C balance between fluxes under climate warming^{36,53–55}.

How do thermal adaptations in $T_{\text{opt}}^{\text{ER}}$ impact ER? Previous studies have focused only on the thermal adaptation of the optimum temperature, but the changes in the corresponding carbon fluxes associated with thermal adaptation have not been carefully examined^{7,27}. The nonlinear relationships between $T_{\text{opt}}^{\text{ER}}$ and annual ER suggested that ER first increases with $T_{\text{opt}}^{\text{ER}}$ when $T_{\text{opt}}^{\text{ER}}$ is below 21.0 °C and then decreases above 21.0 °C (Fig. 5). These results confirmed our fourth hypothesis that ER is closely related with $T_{\text{opt}}^{\text{ER}}$. Traditionally, ecosystem adaptation is often regarded as adjustments in ER that improve the performance of these processes at the new growth temperature^{56,57}. Nevertheless, the concave relationships shown in Fig. 5 implied that higher $T_{\text{opt}}^{\text{ER}}$ does not always lead to higher ER⁵⁸. ER decreases once $T_{\text{opt}}^{\text{ER}}$ is beyond the threshold of 21.0 °C (Fig. 5). Therefore, modelling ER and its adaptation under future climate warming should take into account not only shifts in $T_{\text{opt}}^{\text{ER}}$ but also varying ER associated with dynamic optimum temperature.

Compared with the Farquhar biochemical model of photosynthesis, most approaches to modelling respiration are empirical since respiration is composed of a series of many biochemical processes occurring continuously in all tissues of the ecosystem, with different mechanisms and different metabolic relations^{59,60}. Linking respiration to photosynthesis seems to simplify the respiration models and has also been proposed and widely debated in previous studies⁶¹. By providing strong evidence of the close correlations between the thermal adaptation of ER and GPP across multiple sites and different vegetation types, this study implies a potential approach to explicitly predict the response of respiration to climate change by linking thermal adaptation of respiration to photosynthesis adaptation functions. Meanwhile, our results raise some rather crucial questions for future study. For example, under what conditions would the thermal adaptation of ER be implicitly accompanied by an adaptation response of GPP? What are the mechanisms underlying the widespread thermal adaptation of ER? What role do the differential responses of autotrophic and heterotrophic respiration to increasing temperature play in regulating the optimum temperature of ER? Addressing these issues can help elucidate when and why thermal adaptation of ER happens and can assist in the development of better respiration models.

Methods

FLUXNET data and related variables

The daily mean eddy-covariance carbon fluxes and meteorological data were obtained from FLUXNET datasets (<https://fluxnet.org/>). The FLUXNET datasets were quality controlled, filtered, gap-filled

and partitioned using consistent methods⁶². To avoid self-correlation between GPP and ER induced by flux partitioning of eddy-covariance CO₂ fluxes⁶³, we used ER data and GPP data based on the daytime approach⁶⁴. Only data with all three carbon fluxes (GPP, ER and net ecosystem productivity (NEP)), NEE_VUT_REF_QC > 0.8 and entire whole-year meteorological data after gap filling were selected for further analysis. Then sites showing parabolic temperature response curves of ER were used to investigate the optimum temperature of ER. Finally, a total of 212 individual sites with 1,452 site-years of eddy-covariance data were used in this study covering large areas (37.4° S to 74.5° N, Fig. 1 and Supplementary Table 1). According to the International Geosphere-Biosphere Programme, these sites can be divided into 11 plant functional types: deciduous broadleaf forests (DBF), evergreen broadleaf forests (EBF), evergreen needle-leaf forests (ENF), deciduous needle-leaf forest (DNF), mixed forests (MF), open shrublands (OSH), grasslands (GRA), croplands (CRO), savanna (SAV), woody savanna (WSA) and wetlands (WET). SAV and WSA were merged into SAV.

Meteorological variables used in this study included the annual maximum daily temperature (T_{max} , °C), the annual minimum daily temperature (T_{min} , °C), growing season temperature (GST, °C), growing season solar radiation (GSR), vapour pressure deficit (VPD, kPa), mean annual temperature (MAT, °C), mean annual precipitation (MAP, mm), soil moisture (SM, v/v) and aridity index (AI). SM at 5 cm was obtained from the observation data of each site if available. SM of sites with no observations was extracted from the ESA CCI Soil Moisture Dataset by longitude and latitude (<https://www.esa-soilmoisture-cci.org/>). AI was calculated as precipitation divided by potential evapotranspiration. Potential evapotranspiration was calculated by using the Thornthwaite method based on measured data at each site. All the above variables were calculated from each of the site-year data and then averaged over the years of observation by site.

Besides these meteorological variables, the soil properties and biomass data for each site were extracted from global datasets according to its latitude and longitude. Soil organic carbon (SOC, %), soil bulk density (BD, kg dm⁻³), clay fraction (Clay, %) and soil pH (pH) were retrieved from the Regridded Harmonized World Soil Database v.1.2 in the Oak Ridge National Laboratory Distributed Active Archive Center for Biogeochemical Dynamics (<https://daac.ornl.gov/SOILS/guides/HWSD.html>); aboveground biomass (Biomass, Mg ha⁻¹) was accessed at http://wald.anu.edu.au/data_services/data/global-above-ground-biomass-carbon-v1-0/.

Temperature response curve of ER

The growing season was determined according to whether the average daily air temperature (T_a) was above 5 °C for at least five consecutive days. For each site-year, the daily mean air temperatures and corresponding carbon fluxes (GPP and ER) were binned by 1 °C. The daily air temperature and the corresponding carbon fluxes in each temperature bin were averaged when constructing the ER– T_a or GPP– T_a response curves following previously developed methods⁷. Among the 212 sites, 183 sites followed a similar parabolic response pattern of ER to temperature as shown in Extended Data Fig. 1; we randomly selected a site-year from each vegetation type to show a representative curve.

To further quantitatively test the shape of the ER– T_a curve for each site-year, we fitted a quadratic function using equation (1). $T_{\text{opt}}^{\text{ER}}$ and ER_{max} are the vertex of the parabola. a is parameter estimate of the fitted quadratic function and indicates the direction and extent of curvature. Negative values of a indicate that the curve is concave.

$$\text{ER} = a(T - T_{\text{opt}}^{\text{ER}})^2 + \text{ER}_{\text{max}} \quad (1)$$

Considering that T_a , VPD, solar radiation, SM and LAI are closely correlated and always co-vary with each other, we evaluated the potential impacts of SM, VPD, global radiation (R_g) and LAI when the T_a impact

on ER was analysed. The non-significant relationships between SM, VPD, R_g or LAI and the residuals of ER– T_a regression suggest that the existence of T_{opt}^{ER} was not likely induced by the effects of these confounding factors (Supplementary Fig. 1). LAI data for each site were extracted from global datasets (<https://www.ncei.noaa.gov/products/climate-data-records/leaf-area-index-and-fapar>) according to its latitude and longitude.

For the 29 sites where a T_{opt}^{ER} was absent, we further analysed temperature responses of ER and GPP and constructed the curves site by site, finding that they were mainly due to negligible seasonal temperature variations and the absence of T_{opt}^{GPP} (Supplementary Fig. 2).

Derivation of T_{opt}^{ER} or T_{opt}^{GPP}

The 183 sites that showed parabolic temperature response curves of ER were used to derive T_{opt}^{ER} and investigate the thermal optimality of ER. We defined the peak value of the T_a –ER or T_a –GPP curve as ER_{max} or GPP_{max} , and the corresponding T_a for the peak ER or GPP as the apparent optimum temperature (T_{opt}^{ER} or T_{opt}^{GPP}) of ER or GPP, respectively (Extended Data Fig. 1). We also used the medians of the daily air temperature and the corresponding carbon fluxes in each temperature bin when we constructed the ER– T_a or GPP– T_a response curves. The T_{opt}^{ER} or T_{opt}^{GPP} derived from using median values showed results similar to those derived from using mean values (Supplementary Fig. 3). So, we used T_{opt}^{ER} or T_{opt}^{GPP} derived from using mean values thereafter in this study.

Factors controlling the variation in T_{opt}^{ER} across sites

We investigated the factors influencing the variation in T_{opt}^{ER} across sites (Fig. 3a and Extended Data Fig. 3). The abiotic and biotic factors included T_{max} , T_{min} , GST, VPD, MAT, MAP, AI, GSR, soil pH, SM, SOC, BD, biomass and T_{opt}^{GPP} . To solve the collinearity problem of co-varying climate factors and determine the relative importance of each factor on T_{opt}^{ER} , we used ridge regression to examine the relationship between T_{opt}^{ER} and biotic or abiotic variables and identify the dominant factors determining T_{opt}^{ER} . The ridge regression, by design, solves the problem of collinearity of co-variables and can evaluate the relative importance of each factor independently of T_{opt}^{ER} . Further, we used variation partitioning analysis in R software to quantify the contribution percentage of different variables to the variations in T_{opt}^{ER} (Supplementary Fig. 4).

Temporal variations in T_{opt}^{ER} within sites

To get an understanding of temporal variations in T_{opt}^{ER} across years within sites, we analysed 15 long-term FLUXNET sites with more than 10 years observation data to investigate the thermal acclimation for T_{opt}^{ER} and its relationship with T_{max} and T_{opt}^{GPP} at temporal scale within each site (Supplementary Table 2). The results showed that T_{opt}^{ER} was positively correlated with T_{max} , and the close relationships between T_{opt}^{ER} and T_{opt}^{GPP} also existed over years within sites and across sites (Extended Data Fig. 4).

The adaptation magnitude of T_{opt}^{ER} or T_{opt}^{GPP}

The adaptation magnitude of T_{opt}^{ER} or T_{opt}^{GPP} for each vegetation type was calculated as the slope between T_{opt}^{ER} or T_{opt}^{GPP} and T_{max} , averaged over the years of observation by site. The slope represents the vegetation's capability to keep pace with temperature changes. Slopes (including 95% confidence intervals (CI)) less than 1 indicate that the T_{opt}^{ER} or T_{opt}^{GPP} of these vegetation types cannot fully adapt to T_{max} . Slopes and 95% CIs overlapping with 1 indicate that the T_{opt}^{ER} or T_{opt}^{GPP} of these vegetation types can fully adapt to T_{max} .

Upscaling and uncertainty analysis

To upscale T_{opt}^{ER} at the global scale, we developed a few empirical models. Two thirds of the 183 sites were used for model development, while the remaining sites were used for model validation. We compared the regression results of different regression methods and chose the stepwise regression model with the lowest Akaike information criterion

and highest R^2 to predict current and future T_{opt}^{ER} across the world (Supplementary Table 4). The final selected model included four predictors, including T_{max} , GST, VPD and BD (Supplementary Table 5).

To get the global data of these 4 predictors, we used Climatic Research Unit/National Centers for Environmental Protection (CRU/NCEP) 6-hourly dataset to obtain the air temperature and relative humidity (<https://data.ucar.edu/en/dataset/cruncep-version-7-atmospheric-forcing-data-for-the-community-land-model>). Then we calculated their daily values and extracted the T_{max} , the GST (where the daily air temperature was above 5 °C for at least five consecutive days) and VPD. BD, which we used to simulate current and future T_{opt}^{ER} , was obtained from the Regrided Harmonized World Soil Database v.1.2 in the Oak Ridge National Laboratory Distributed Active Archive Center for Biogeochemical Dynamics (<https://daac.ornl.gov/SOILS/guides/HWSD.html>).

The remaining 29 sites without detected T_{opt}^{ER} were not included in establishing the empirical model because the purpose of the model was to upscale T_{opt}^{ER} , which these 29 sites had not reached yet. We justified that the exclusion of these 29 sites would not impact our upscaling results (Supplementary Fig. 5).

To predict future T_{opt}^{ER} , we used daily air temperature and relative humidity in 2091–2100 from the dataset of Lawrence Livermore National Library (<https://esgf-node.llnl.gov/projects/esgf-llnl/>). We chose the NorESM2-MM model under the SSP2–4.5 scenario from Coupled Model Intercomparison Project 6 to do the prediction.

To assess the uncertainty of the model simulation, we adopted the Latin hypercube sampling-based Monte Carlo method to quantify the uncertainties of the global prediction of current and future T_{opt}^{ER} estimated by the empirical models (Extended Data Fig. 7 and Supplementary Information 5).

Reporting summary

Further information on research design is available in the Nature Portfolio Reporting Summary linked to this article.

Data availability

All FLUXNET data can be downloaded at <https://fluxnet.fluxdata.org>. Soil properties were retrieved from the Regrided Harmonized World Soil Database v.1.2 in the Oak Ridge National Laboratory Distributed Active Archive Center for Biogeochemical Dynamics (<https://daac.ornl.gov/SOILS/guides/HWSD.html>). Biomass data were obtained at http://wald.anu.edu.au/data_services/data/global-above-ground-biomass-carbon-v1-0/. Soil moisture used to extract data for sites without providing soil water conditions was obtained from the European Space Agency's (ESA) Soil Moisture Climate Change Initiative (CCI) project (<https://www.esa-soilmoisture-cci.org/>). Leaf area index data were obtained from <https://www.ncei.noaa.gov/products/climate-data-records/leaf-area-index-and-fapar>. Current air temperature and relative humidity data were obtained from the Climatic Research Unit/National Centers for Environmental Protection (CRU/NCEP) 6-hourly dataset (<https://data.ucar.edu/en/dataset/cruncep-version-7-atmospheric-forcing-data-for-the-community-land-model>). Future daily air temperature and relative humidity data were obtained from the Lawrence Livermore National Library (<https://esgf-node.llnl.gov/projects/esgf-llnl/>).

Code availability

Code used for data analysis in this study is available at https://figshare.com/articles/online_resource/code_docx/23514492.

References

- Wenzel, S., Eyring, V., Gerber, E. P. & Karpechko, A. Y. Constraining future summer austral jet stream positions in the CMIP5 ensemble by process-oriented multiple diagnostic regression. *J. Clim.* **29**, 673–687 (2016).

2. Valentini, R. et al. Respiration as the main determinant of carbon balance in European forests. *Nature* **404**, 861–865 (2000).
3. Lloyd, J. & Taylor, J. A. On the temperature dependence of soil respiration. *Funct. Ecol.* **8**, 315–323 (1994).
4. Farquhar, G. D., von Caemmerer, S. & Berry, J. A. A biochemical model of photosynthetic CO₂ assimilation in leaves of C₃ species. *Planta* **149**, 78–90 (1980).
5. Smith, N. G. & Keenan, T. F. Mechanisms underlying leaf photosynthetic acclimation to warming and elevated CO₂ as inferred from least-cost optimality theory. *Glob. Chang. Biol.* **26**, 5202–5216 (2020).
6. Smith, N. G. & Dukes, J. S. Plant respiration and photosynthesis in global-scale models: incorporating acclimation to temperature and CO₂. *Glob. Chang. Biol.* **19**, 45–63 (2013).
7. Niu, S. et al. Thermal optimality of net ecosystem exchange of carbon dioxide and underlying mechanisms. *New Phytol.* **194**, 775–783 (2012).
8. Lombardozzi, D. L., Bonan, G. B., Smith, N. G., Dukes, J. S. & Fisher, R. A. Temperature acclimation of photosynthesis and respiration: a key uncertainty in the carbon cycle-climate feedback. *Geophys. Res. Lett.* **42**, 8624–8631 (2015).
9. Keppel-Aleks, G. et al. Separating the influence of temperature, drought, and fire on interannual variability in atmospheric CO₂. *Glob. Biogeochem. Cycles* **28**, 1295–1310 (2014).
10. Friedlingstein, P. et al. Global carbon budget 2019. *Earth Syst. Sci. Data* **11**, 1783–1838 (2019).
11. Niu, B. et al. Warming homogenizes apparent temperature sensitivity of ecosystem respiration. *Sci. Adv.* **7**, eabc7358 (2021).
12. Mahecha, M. et al. Global convergence in the temperature sensitivity of respiration at ecosystem level. *Science* **329**, 838–840 (2010).
13. Crous, K. Y., Uddling, J. & De Kauwe, M. G. Temperature responses of photosynthesis and respiration in evergreen trees from boreal to tropical latitudes. *New Phytol.* **234**, 353–374 (2022).
14. Smith, N. G. & Dukes, J. S. Short-term acclimation to warmer temperatures accelerates leaf carbon exchange processes across plant types. *Glob. Chang. Biol.* **23**, 4840–4853 (2017).
15. O’Sullivan, O. S. et al. High-resolution temperature responses of leaf respiration in snow gum (*Eucalyptus pauciflora*) reveal high-temperature limits to respiratory function. *Plant Cell Environ.* **36**, 1268–1284 (2013).
16. Heskel, M. A. et al. Convergence in the temperature response of leaf respiration across biomes and plant functional types. *Proc. Natl Acad. Sci. USA* **113**, 3832–3837 (2016).
17. Atkin, O. K. & Tjoelker, M. G. Thermal acclimation and the dynamic response of plant respiration to temperature. *Trends Plant Sci.* **8**, 343–351 (2003).
18. Vanderwel, M. C. et al. Global convergence in leaf respiration from estimates of thermal acclimation across time and space. *New Phytol.* **207**, 1026–1037 (2015).
19. Liang, L. L. et al. Macromolecular rate theory (MMRT) provides a thermodynamics rationale to underpin the convergent temperature response in plant leaf respiration. *Glob. Chang. Biol.* **24**, 1538–1547 (2018).
20. Fanin, N. et al. Soil enzymes in response to climate warming: mechanisms and feedbacks. *Funct. Ecol.* **36**, 1378–1395 (2022).
21. Yang, Z. et al. Recent photosynthates are the primary carbon source for soil microbial respiration in subtropical forests. *Geophys. Res. Lett.* **49**, e2022GL101147 (2022).
22. Tian, W. et al. Thermal adaptation occurs in the respiration and growth of widely distributed bacteria. *Glob. Chang. Biol.* **28**, 2820–2829 (2022).
23. Yamori, W., Hikosaka, K. & Way, D. A. Temperature response of photosynthesis in C₃, C₄, and CAM plants: temperature acclimation and temperature adaptation. *Photosynth. Res.* **119**, 101–117 (2014).
24. Sendall, K. M. et al. Acclimation of photosynthetic temperature optima of temperate and boreal tree species in response to experimental forest warming. *Glob. Chang. Biol.* **21**, 1342–1357 (2015).
25. Sage, R. F. & Kubien, D. S. The temperature response of C₃ and C₄ photosynthesis. *Plant Cell Environ.* **30**, 1086–1106 (2007).
26. Niu, S. et al. Climatic warming changes plant photosynthesis and its temperature dependence in a temperate steppe of northern China. *Environ. Exp. Bot.* **63**, 91–101 (2008).
27. Huang, M. et al. Air temperature optima of vegetation productivity across global biomes. *Nat. Ecol. Evol.* **3**, 772–779 (2019).
28. Way, D. A. & Yamori, W. Thermal acclimation of photosynthesis: on the importance of adjusting our definitions and accounting for thermal acclimation of respiration. *Photosynth. Res.* **119**, 89–100 (2014).
29. Wright, I. J. et al. The worldwide leaf economics spectrum. *Nature* **428**, 821–827 (2004).
30. Tcherkez, G., Boex-Fontvieille, E., Mahé, A. & Hodges, M. Respiratory carbon fluxes in leaves. *Curr. Opin. Plant Biol.* **15**, 308–314 (2012).
31. O’Leary, B. M., Asao, S., Millar, A. H. & Atkin, O. K. Core principles which explain variation in respiration across biological scales. *New Phytol.* **222**, 670–686 (2019).
32. Noguchi, K. & Yoshida, K. Interaction between photosynthesis and respiration in illuminated leaves. *Mitochondrion* **8**, 87–99 (2008).
33. Hoefnagel, M. H. N., Atkin, O. K. & Wiskich, J. T. Interdependence between chloroplasts and mitochondria in the light and the dark. *Biochim. Biophys. Acta Bioenerg.* **1366**, 235–255 (1998).
34. Hogberg, P. et al. Large-scale forest girdling shows that current photosynthesis drives soil respiration. *Nature* **411**, 789–792 (2001).
35. Hartley, I. P. et al. The dependence of respiration on photosynthetic substrate supply and temperature: integrating leaf, soil and ecosystem measurements. *Glob. Chang. Biol.* **12**, 1954–1968 (2006).
36. Ziska, L. H. & Bunce, J. A. The influence of increasing growth temperature and CO₂ concentration on the ratio of respiration to photosynthesis in soybean seedlings. *Glob. Chang. Biol.* **4**, 637–643 (1998).
37. Waring, R. H., Landsberg, J. J. & Williams, M. Net primary production of forests: a constant fraction of gross primary production? *Tree Physiol.* **18**, 129–134 (1998).
38. Van Oijen, M., Schapendonk, A. & Hoglind, M. On the relative magnitudes of photosynthesis, respiration, growth and carbon storage in vegetation. *Ann. Bot.* **105**, 793–797 (2010).
39. Gifford, R. M. Plant respiration in productivity models: conceptualisation, representation and issues for global terrestrial carbon-cycle research. *Funct. Plant Biol.* **30**, 171–186 (2003).
40. Loveys, B. R., Scheurwater, I., Pons, T. L., Fitter, A. H. & Atkin, O. K. Growth temperature influences the underlying components of relative growth rate: an investigation using inherently fast- and slow-growing plant species. *Plant Cell Environ.* **25**, 975–987 (2002).
41. Loveys, B. R. et al. Thermal acclimation of leaf and root respiration: an investigation comparing inherently fast- and slow-growing plant species. *Glob. Chang. Biol.* **9**, 895–910 (2003).
42. Atkin, O. K., Cheurwater, I. & Pons, T. L. High thermal acclimation potential of both photosynthesis and respiration in two lowland *Plantago* species in contrast to an alpine congeneric. *Glob. Chang. Biol.* **12**, 500–515 (2006).
43. Atkin, O. K., Bruhn, D., Hurry, V. M. & Tjoelker, M. G. The hot and the cold: unravelling the variable response of plant respiration to temperature. *Funct. Plant Biol.* **32**, 87–105 (2005).
44. Wang, H. et al. Acclimation of leaf respiration consistent with optimal photosynthetic capacity. *Glob. Chang. Biol.* **26**, 2573–2583 (2020).

45. Dusenage, M. E., Madhavji, S. & Way, D. A. Contrasting acclimation responses to elevated CO₂ and warming between an evergreen and a deciduous boreal conifer. *Glob. Chang. Biol.* **26**, 3639–3657 (2020).
46. Dacal, M., Bradford, M. A., Plaza, C., Maestre, F. T. & García-Palacios, P. Soil microbial respiration adapts to ambient temperature in global drylands. *Nat. Ecol. Evol.* **3**, 232–238 (2019).
47. Smith, N. G., Malyshev, S. L., Shevliakova, E., Kattge, J. & Dukes, J. S. Foliar temperature acclimation reduces simulated carbon sensitivity to climate. *Nat. Clim. Change* **6**, 407–411 (2015).
48. Huntingford, C. et al. Implications of improved representations of plant respiration in a changing climate. *Nat. Commun.* **8**, 1602 (2017).
49. Alvarez, G. et al. Catalytic power of enzymes decreases with temperature: new insights for understanding soil C cycling and microbial ecology under warming. *Glob. Chang. Biol.* **24**, 4238–4250 (2018).
50. Duffy, K. A. et al. How close are we to the temperature tipping point of the terrestrial biosphere? *Sci. Adv.* **7**, eaay1052 (2020).
51. Atkin, O. K. et al. Using temperature-dependent changes in leaf scaling relationships to quantitatively account for thermal acclimation of respiration in a coupled global climate-vegetation model. *Glob. Chang. Biol.* **14**, 2709–2726 (2008).
52. Janzen, D. H. Why mountain passes are higher in tropics. *Am. Nat.* **101**, 233–249 (1967).
53. Stitt, M. & Hurry, V. A plant for all seasons: alterations in photosynthetic carbon metabolism during cold acclimation in *Arabidopsis*. *Curr. Opin. Plant Biol.* **5**, 199–206 (2002).
54. Gifford, R. M. Whole plant respiration and photosynthesis of wheat under increased CO₂ concentration and temperature-long-term vs short-term distinctions for modelling. *Glob. Chang. Biol.* **1**, 385–396 (1995).
55. Dewar, R. C., Medlyn, B. E. & Mcmurtrie, R. E. Acclimation of the respiration/photosynthesis ratio to temperature: insights from a model. *Glob. Chang. Biol.* **5**, 615–622 (1999).
56. Lambers, H., Chapin, F. S. & Pons, T. L. *Plant Physiological Ecology* (Springer, 1998).
57. Korner, C. & Larcher, W. Plant life in cold climates. *Symp. Soc. Exp. Biol.* **42**, 25–57 (1988).
58. Atkin, O. K. et al. Global variability in leaf respiration in relation to climate, plant functional types and leaf traits. *New Phytol.* **206**, 614–636 (2015).
59. Ryan, M. G. & Asao, S. Clues for our missing respiration model. *New Phytol.* **222**, 1167–1170 (2019).
60. Reich, P. B. The carbon dioxide exchange. *Science* **329**, 774–775 (2010).
61. Collalti, A. & Prentice, I. C. Is NPP proportional to GPP? Waring's hypothesis 20 years on. *Tree Physiol.* **39**, 1473–1483 (2019).
62. Pastorello, G. et al. The FLUXNET2015 dataset and the ONEFlux processing pipeline for eddy covariance data. *Sci. Data* **7**, 225 (2020).
63. Vickers, D., Thomas, C. K., Martin, J. G. & Law, B. Self-correlation between assimilation and respiration resulting from flux partitioning of eddy-covariance CO₂ fluxes. *Agric. For. Meteorol.* **149**, 1552–1555 (2009).
64. Lasslop, G. et al. Separation of net ecosystem exchange into assimilation and respiration using a light response curve approach: critical issues and global evaluation. *Glob. Chang. Biol.* **16**, 187–208 (2010).

Acknowledgements

This study was financially supported by the National Natural Science Foundation of China (31988102), the National Key Technology R & D Program of China (2022YFF0802102) and the International Partnership Program of the Chinese Academy of Science (177GJHZ2022020BS). We used the eddy-covariance data of the FLUXNET community by the following networks: AmeriFlux, AfriFlux, AsiaFlux, CarboAfrica, CarboEuropeIP, CarboItaly, CarboMont, ChinaFlux, Fluxnet-Canada, GreenGrass, ICOS, KoFlux, LBA, NECC, OzFlux-TERN, TCOS-Siberia, Swiss FluxNet and USCCC. The ERA-Interim reanalysis data were provided by ECMWF and processed by Laboratoire des sciences du climat et de l'environnement (LSCE). The FLUXNET eddy-covariance data processing and harmonization was carried out by the European Fluxes Database Cluster and the AmeriFlux Management Project (with support by European Union H2020 projects and the US Department of Energy Office of Science, respectively), with contributions from the Carbon Dioxide Information Analysis Center, ICOS Ecosystem Thematic Centre, and OzFlux, ChinaFlux and AsiaFlux offices.

Author contributions

W.C. and S.N. conceived the ideas and designed the study. W.C. and S.W. collected and analysed the data. W.C. and S.N. wrote the first draft of the manuscript. J.W., J.X., Y.L. and G.Y. offered thoughts on the analysis and contributed critically to the writing through multiple rounds of revisions.

Competing interests

The authors declare no competing interests.

Additional information

Extended data is available for this paper at <https://doi.org/10.1038/s41559-023-02121-w>.

Supplementary information The online version contains supplementary material available at <https://doi.org/10.1038/s41559-023-02121-w>.

Correspondence and requests for materials should be addressed to Shuli Niu.

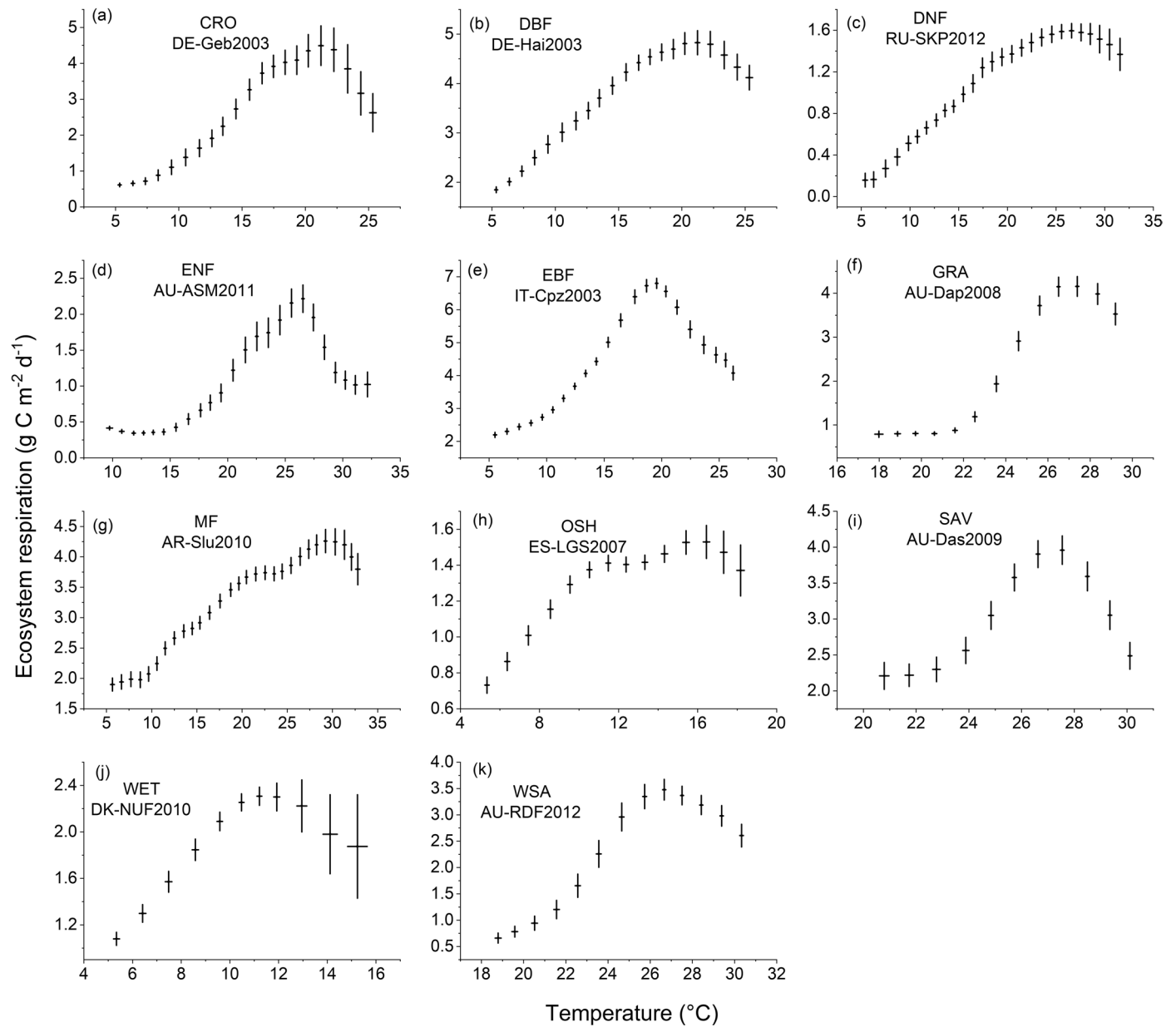
Peer review information *Nature Ecology & Evolution* thanks Kristine Crous and the other, anonymous, reviewer(s) for their contribution to the peer review of this work.

Reprints and permissions information is available at www.nature.com/reprints.

Publisher's note Springer Nature remains neutral with regard to jurisdictional claims in published maps and institutional affiliations.

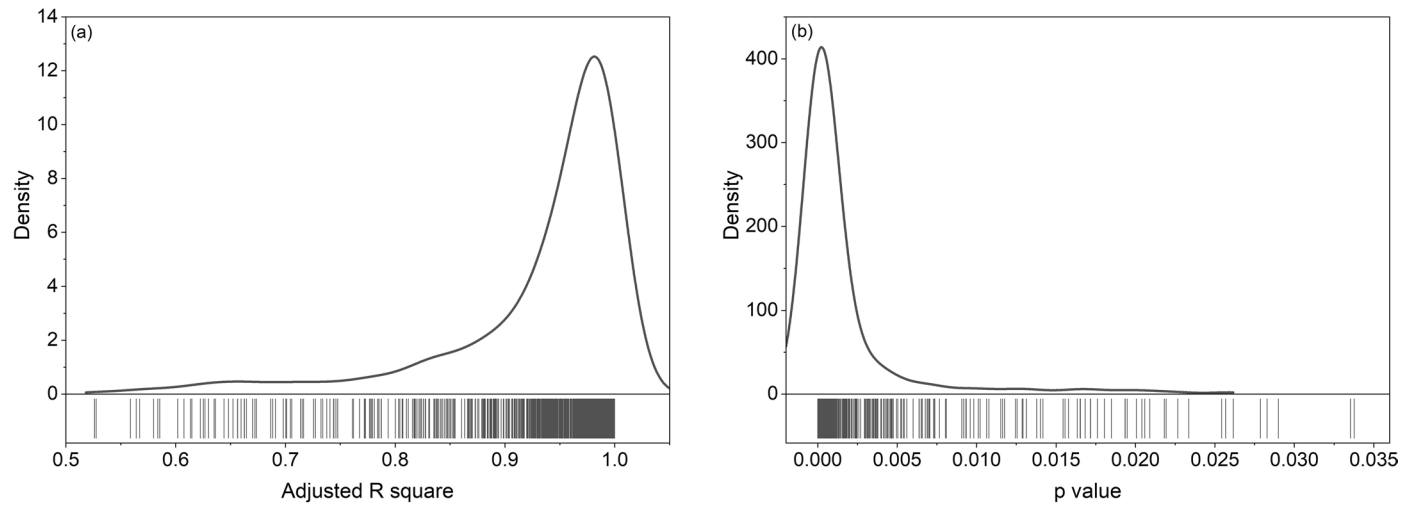
Springer Nature or its licensor (e.g. a society or other partner) holds exclusive rights to this article under a publishing agreement with the author(s) or other rightsholder(s); author self-archiving of the accepted manuscript version of this article is solely governed by the terms of such publishing agreement and applicable law.

© The Author(s), under exclusive licence to Springer Nature Limited 2023

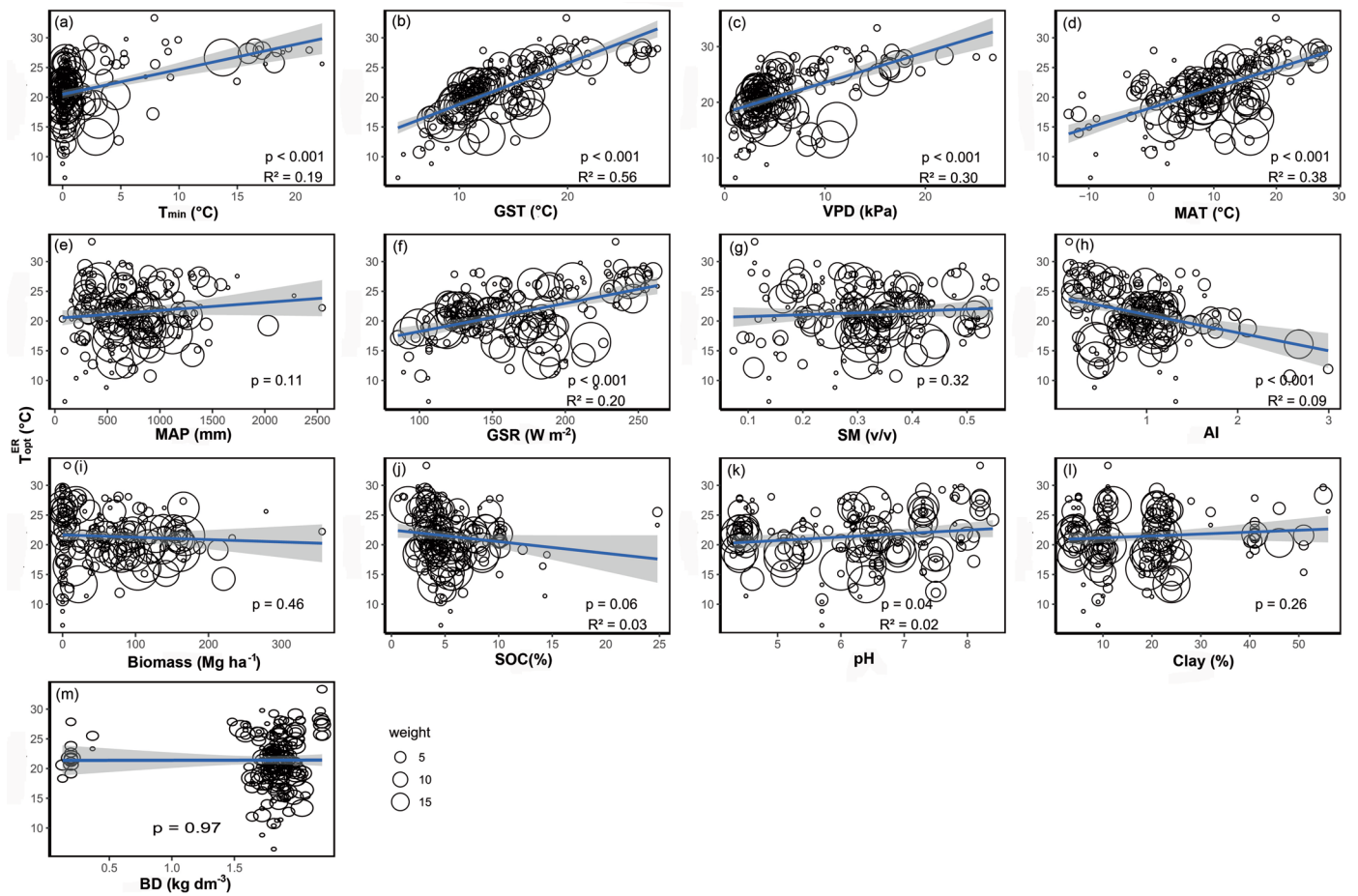


Extended Data Fig. 1 | Response of ecosystem respiration (ER) to daily temperature at the 11 sites from 11 different vegetation types. Points and Error bars indicate mean \pm s.d. for each temperature bin. The vegetation types are as follows: (a) croplands (CRO), (b) deciduous broadleaf forests (DBF),

(c) deciduous needle-leaf forest (DNF), (d) evergreen needle leaf forests (ENF), (e) evergreen broadleaf forests (EBF), (f) grasslands (GRA), (g) mixed forests (MF), (h) opened shrublands (OSH), (i) savanna (SAV), (j) wetlands (WET), (k) woody savanna (WSA).

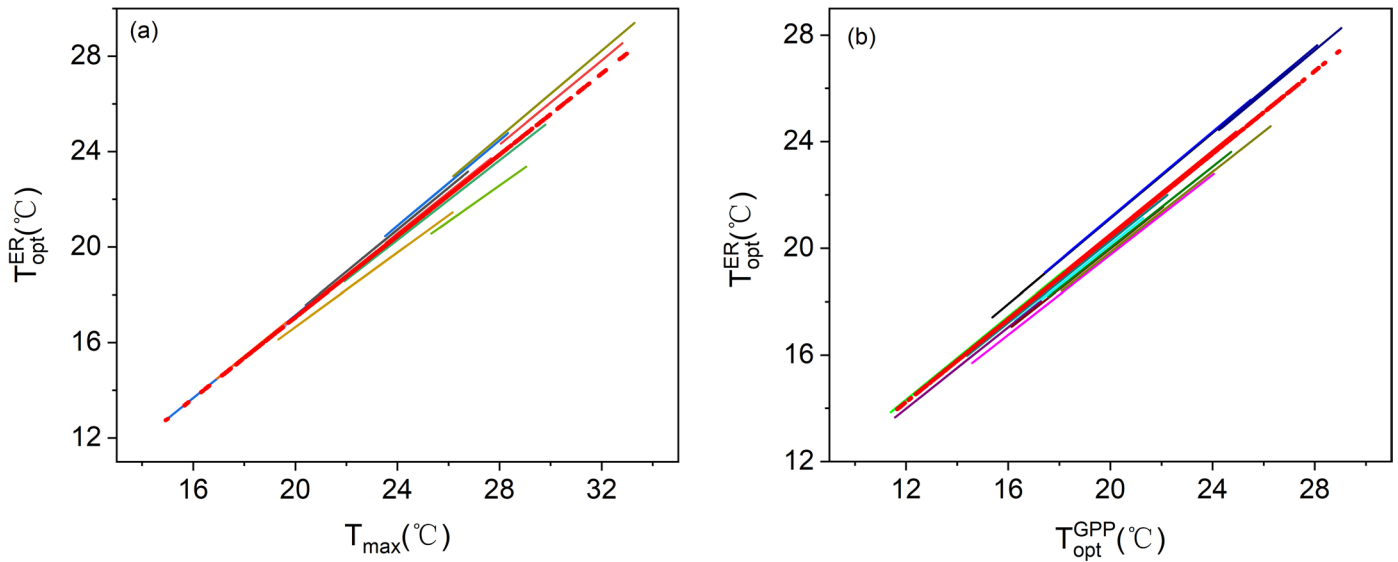


Extended Data Fig. 2 | Goodness-of-fit of the fitted quadratic function at T_{opt}^{ER} for the 183 sites with temperature optima. (a) Distribution of adjusted R square of the fitted quadratic function. **(b)** Distribution of P value of the fitted quadratic function at the 0.05 level.

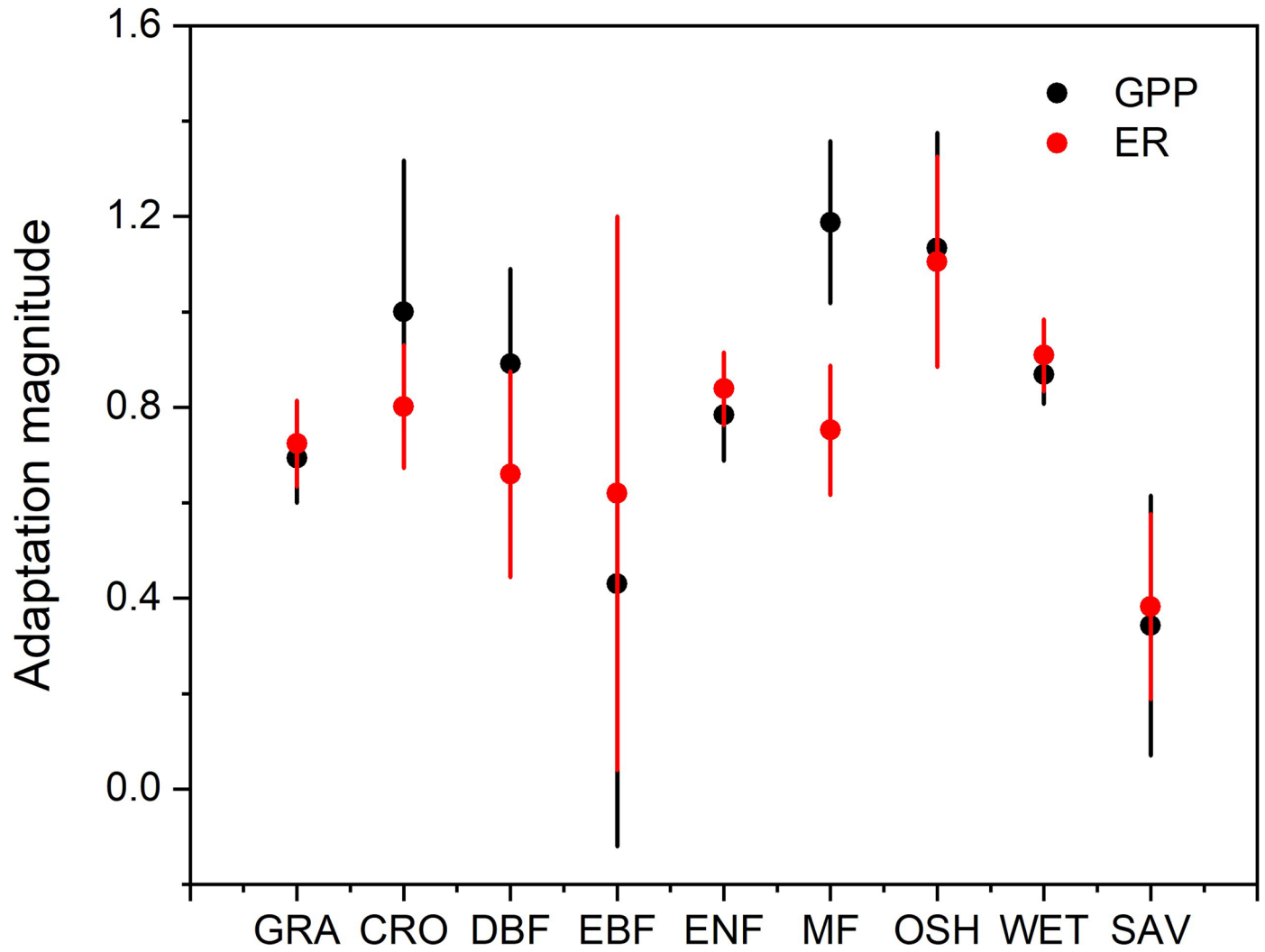


Extended Data Fig. 3 | Bivariate plots between T_{opt}^{ER} and influencing variables. Symbol point size is proportional to numbers of site-years in each site. The influencing variables are as follows: (a) annual minimum daily temperature (T_{min} , °C); (b) growing season temperature (GST, °C); (c) vapor pressure deficit (VPD, kPa); (d) mean annual temperature (MAT, °C); (e) mean annual precipitation (MAP,

$mm yr^{-1}$); (f) global solar radiation (GSR, W/m^2); (g) soil moisture (SM); (h) aridity index (AI); (i) aboveground biomass (Biomass, $Mg ha^{-1}$), soil growing season temperature (GST, °C); vapor pressure deficit (VPD, kPa); soil moisture (SM); aridity index (AI); aboveground biomass (Biomass, $Mg ha^{-1}$), (j) soil organic carbon (SOC, %), (k) soil pH (pH), (l) clay fraction (Clay, %) (m) soil bulk density (BD, $kg dm^{-3}$).



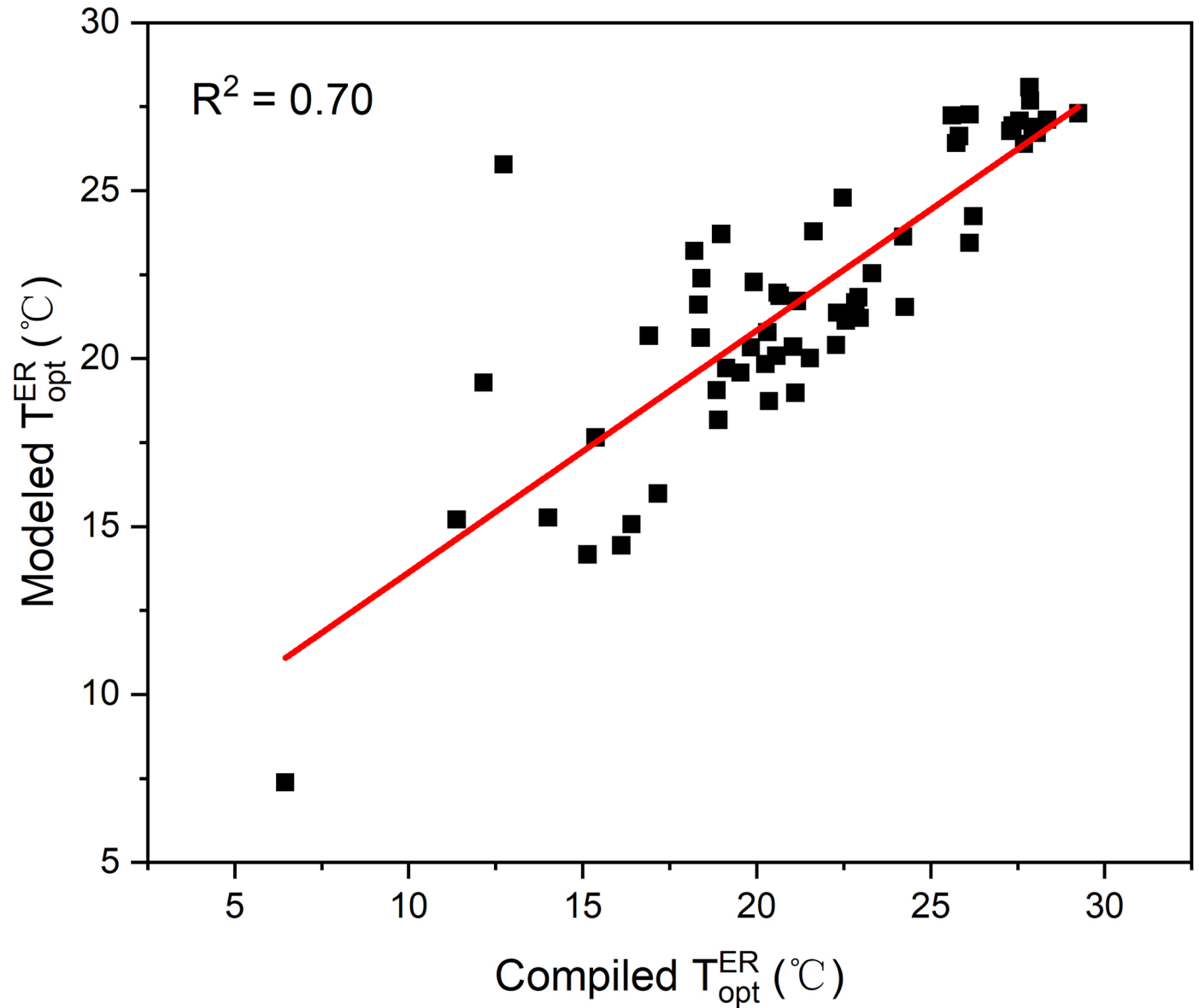
Extended Data Fig. 4 | The relationship of T_{opt}^{ER} with maximum temperature (T_{max}) (a) and T_{opt}^{GPP} (b) across years at the 15 sites with > 10 years of data. Each colored line indicates one site. The red dotted line was the fixed-effect linear regression slope between sites considering site-level random effects estimated from the linear-mixed model.



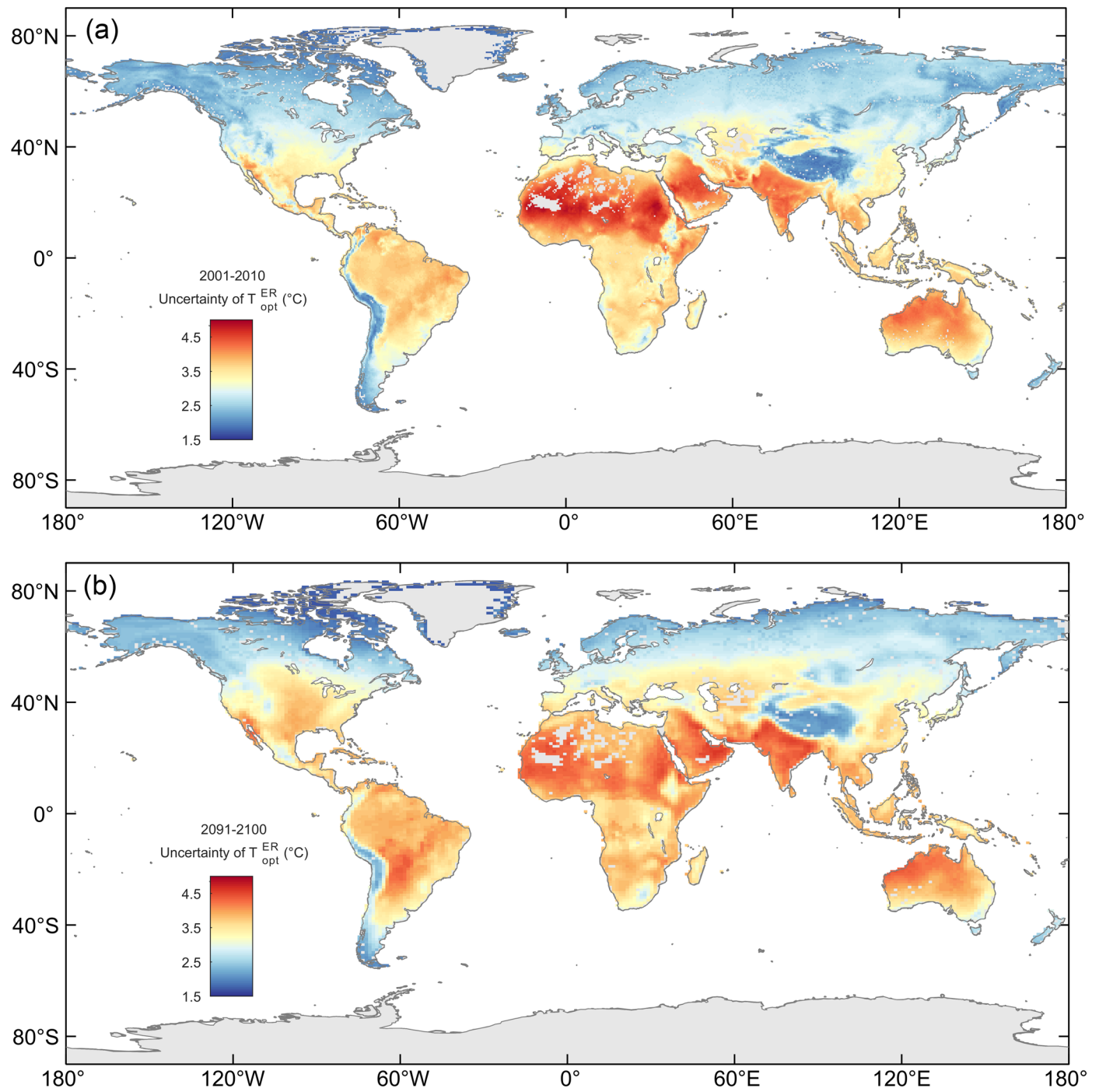
Extended Data Fig. 5 | Adaptation magnitude of GPP and ER among different vegetation types. The adaptation magnitude of T_{opt}^{ER} or T_{opt}^{GPP} was calculated as the slope between T_{opt}^{ER} or T_{opt}^{GPP} and T_{max} . The vegetation types are as follows: croplands (CRO, $n = 17$), deciduous broadleaf forests (DBF, $n = 22$), evergreen

needle leaf forests (ENF, $n = 45$), evergreen broadleaf forests (EBF, $n = 10$), grasslands (GRA, $n = 35$), mixed forests (MF, $n = 8$), opened shrublands (OSH, $n = 14$), wetlands (WET, $n = 17$) and savanna (SAV, $n = 13$). Points and error bars indicate mean \pm 95% confidence intervals.

Validation of the empirical model



Extended Data Fig. 6 | Comparison of modeled T_{opt}^{ER} with the compiled T_{opt}^{ER} ($R^2 = 0.70$; $P < 0.001$).



Extended Data Fig. 7 | Uncertainty of global estimation of T_{opt}^{ER} with an empirical model. (a) Current uncertainty. (b) Future uncertainty under SSP2-4.5 scenario.

Reporting Summary

Nature Portfolio wishes to improve the reproducibility of the work that we publish. This form provides structure for consistency and transparency in reporting. For further information on Nature Portfolio policies, see our [Editorial Policies](#) and the [Editorial Policy Checklist](#).

Statistics

For all statistical analyses, confirm that the following items are present in the figure legend, table legend, main text, or Methods section.

- | n/a | Confirmed |
|-------------------------------------|--|
| <input type="checkbox"/> | <input checked="" type="checkbox"/> The exact sample size (n) for each experimental group/condition, given as a discrete number and unit of measurement |
| <input type="checkbox"/> | <input checked="" type="checkbox"/> A statement on whether measurements were taken from distinct samples or whether the same sample was measured repeatedly |
| <input type="checkbox"/> | <input checked="" type="checkbox"/> The statistical test(s) used AND whether they are one- or two-sided
<i>Only common tests should be described solely by name; describe more complex techniques in the Methods section.</i> |
| <input checked="" type="checkbox"/> | <input type="checkbox"/> A description of all covariates tested |
| <input checked="" type="checkbox"/> | <input type="checkbox"/> A description of any assumptions or corrections, such as tests of normality and adjustment for multiple comparisons |
| <input type="checkbox"/> | <input checked="" type="checkbox"/> A full description of the statistical parameters including central tendency (e.g. means) or other basic estimates (e.g. regression coefficient) AND variation (e.g. standard deviation) or associated estimates of uncertainty (e.g. confidence intervals) |
| <input type="checkbox"/> | <input checked="" type="checkbox"/> For null hypothesis testing, the test statistic (e.g. F , t , r) with confidence intervals, effect sizes, degrees of freedom and P value noted
<i>Give P values as exact values whenever suitable.</i> |
| <input checked="" type="checkbox"/> | <input type="checkbox"/> For Bayesian analysis, information on the choice of priors and Markov chain Monte Carlo settings |
| <input checked="" type="checkbox"/> | <input type="checkbox"/> For hierarchical and complex designs, identification of the appropriate level for tests and full reporting of outcomes |
| <input checked="" type="checkbox"/> | <input type="checkbox"/> Estimates of effect sizes (e.g. Cohen's d , Pearson's r), indicating how they were calculated |

Our web collection on [statistics for biologists](#) contains articles on many of the points above.

Software and code

Policy information about [availability of computer code](#)

Data collection

Data analysis

For manuscripts utilizing custom algorithms or software that are central to the research but not yet described in published literature, software must be made available to editors and reviewers. We strongly encourage code deposition in a community repository (e.g. GitHub). See the Nature Portfolio [guidelines for submitting code & software](#) for further information.

Data

Policy information about [availability of data](#)

All manuscripts must include a [data availability statement](#). This statement should provide the following information, where applicable:

- Accession codes, unique identifiers, or web links for publicly available datasets
- A description of any restrictions on data availability
- For clinical datasets or third party data, please ensure that the statement adheres to our [policy](#)

All FLUXNET data can be downloaded at: <https://fluxnet.fluxdata.org>. Soil properties were retrieved from the Re-gridded Harmonized World Soil Database v1.2 in the Oak Ridge National Laboratory Distributed Active Archive Center for Biogeochemical Dynamics (<https://daac.ornl.gov/SOILS/guides/HWSD.html>). Biomass data were obtained at http://wald.anu.edu.au/data_services/data/global-above-ground-biomass-carbon-v1-0/. Soil moisture used to extract data for sites without

providing soil water conditions was obtained from the European Space Agency's (ESA) Soil Moisture Climate Change Initiative (CCI) project (<https://www.esa-soilmoisture-cci.org/>). Leaf area index data were obtained at <https://www.ncei.noaa.gov/products/climate-data-records/leaf-area-index-and-fapar>. Current air temperature and relative humidity data was obtained from the Climatic Research Unit/National Centers for Environmental Protection (CRU/NCEP) 6-hourly dataset (<https://data.ucar.edu/en/dataset/cruncep-version-7-atmospheric-forcing-data-for-the-community-land-model>). And future daily air temperature and relative humidity data was obtained from Lawrence Livermore National Library (<https://esgf-node.llnl.gov/projects/esgf-llnl/>).

Research involving human participants, their data, or biological material

Policy information about studies with [human participants or human data](#). See also policy information about [sex, gender \(identity/presentation\), and sexual orientation](#) and [race, ethnicity and racism](#).

Reporting on sex and gender	N/A
Reporting on race, ethnicity, or other socially relevant groupings	N/A
Population characteristics	N/A
Recruitment	N/A
Ethics oversight	N/A

Note that full information on the approval of the study protocol must also be provided in the manuscript.

Field-specific reporting

Please select the one below that is the best fit for your research. If you are not sure, read the appropriate sections before making your selection.

Life sciences Behavioural & social sciences Ecological, evolutionary & environmental sciences

For a reference copy of the document with all sections, see nature.com/documents/nr-reporting-summary-flat.pdf

Ecological, evolutionary & environmental sciences study design

All studies must disclose on these points even when the disclosure is negative.

Study description	Temperature response curves of ecosystem respiration from 212 globally distributed sites shows widespread evidence for an optimum temperature that is the result of thermal adaptation.
Research sample	The daily eddy-covariance Ecosystem Respiration data were obtained from FLUXNET datasets. A total of 212 individual FLUXNET sites with 1452 site-years of ER data were used in this study. We also used an ensemble of global remote sensing observations. Details can be seen in the Methods section.
Sampling strategy	N/A
Data collection	N/A
Timing and spatial scale	N/A
Data exclusions	N/A
Reproducibility	N/A
Randomization	N/A
Blinding	N/A

Did the study involve field work? Yes No

Reporting for specific materials, systems and methods

We require information from authors about some types of materials, experimental systems and methods used in many studies. Here, indicate whether each material, system or method listed is relevant to your study. If you are not sure if a list item applies to your research, read the appropriate section before selecting a response.

Materials & experimental systems

n/a	Included in the study
<input checked="" type="checkbox"/>	<input type="checkbox"/> Antibodies
<input checked="" type="checkbox"/>	<input type="checkbox"/> Eukaryotic cell lines
<input checked="" type="checkbox"/>	<input type="checkbox"/> Palaeontology and archaeology
<input checked="" type="checkbox"/>	<input type="checkbox"/> Animals and other organisms
<input checked="" type="checkbox"/>	<input type="checkbox"/> Clinical data
<input checked="" type="checkbox"/>	<input type="checkbox"/> Dual use research of concern
<input checked="" type="checkbox"/>	<input type="checkbox"/> Plants

Methods

n/a	Included in the study
<input checked="" type="checkbox"/>	<input type="checkbox"/> ChIP-seq
<input checked="" type="checkbox"/>	<input type="checkbox"/> Flow cytometry
<input checked="" type="checkbox"/>	<input type="checkbox"/> MRI-based neuroimaging